

# Statistics of Pressure Fluctuations in Decaying, Isotropic Turbulence

Chirag Kalelkar\*

*Centre for Condensed Matter Theory, Department of Physics,  
Indian Institute of Science, Bangalore 560012, India.*

We present results from a systematic direct-numerical simulation study of pressure fluctuations in an unforced, incompressible, homogeneous, and isotropic, three-dimensional turbulent fluid. At cascade completion, isosurfaces of low pressure are found to be organised as slender filaments, whereas the predominant isostructures appear sheet-like. We exhibit several new results, including plots of probability distributions of the spatial pressure-difference, the pressure-gradient norm, and the eigenvalues of the pressure-hessian tensor. Plots of the temporal evolution of the mean pressure-gradient norm, and the mean eigenvalues of the pressure-hessian tensor are also exhibited. We find the statistically preferred orientations between the eigenvectors of the pressure-hessian tensor, the pressure-gradient, the eigenvectors of the strain-rate tensor, the vorticity, and the velocity. Statistical properties of the non-local part of the pressure-hessian tensor are also exhibited, for the first time. We present numerical tests (in the viscous case) of some conjectures of Ohkitani [Phys. Fluids A **5**, 2570 (1993)] and Ohkitani and Kishiba [Phys. Fluids **7**, 411 (1995)] concerning the pressure-hessian and the strain-rate tensors, for the unforced, incompressible, three-dimensional Euler equations.

PACS numbers: 47.27.Gs

## I. INTRODUCTION

The pressure at a point in an incompressible fluid is a non-local functional of the velocity field, and inherently difficult to measure in laboratory experiments. However, high-resolution direct-numerical simulations (DNS) provide accurate statistics of the pressure field. Pressure fluctuations have been extensively studied in both numerical studies[1, 2, 3, 4, 5, 6] and laboratory experiments[7, 8, 9, 10] of *statistically steady*, homogeneous, and isotropic turbulent flows. High-resolution numerical studies[1, 2, 3, 4] show, that the pressure spectrum exhibits a wavenumber range with power-law scaling, in accordance with predictions from a phenomenological theory due to Kolmogorov[11]. The pressure probability distribution is widely accepted to be negatively skewed, and to exhibit an exponential low-pressure tail[7, 8]. Regions of low pressure are found to be organised as slender filamentary structures in both numerical studies[2] and laboratory experiments[9, 10].

The ‘canonical’ isotropic turbulent flow is a *decaying* turbulent flow behind a grid[11]. The study of decaying turbulence is important since the results are uninfluenced by statistics of the forcing and directly reflect effects of the nonlinear terms in the Navier-Stokes equations (see Eqs. (1) below). In contrast to statistically steady turbulence, systematic numerical studies of pressure fluctuations within the context of decaying, homogeneous, and isotropic turbulence are extremely scarce. The only available work is a low-resolution DNS study due to Schumann and Patterson[12] who exhibited plots of the root-mean-square pressure fluctuations as a func-

tion of the time, and the isosurfaces of low pressure. The low-pressure isosurfaces in this study[12] were shown to be organised as ‘cloud’-like structures, in contrast to the slender filaments seen in DNS studies[2] of statistically steady turbulence at higher resolutions. The pressure-hessian tensor and the pressure-gradient were not studied in this work[12]. In both statistically steady and decaying turbulence, a comprehensive study of possible alignments between vectors of interest in a turbulent flow, namely, the eigenvectors of the pressure-hessian tensor, the pressure-gradient, the eigenvectors of the strain-rate tensor, the vorticity, and the velocity, is entirely lacking. In this paper, we present results from a systematic numerical study of the pressure, the pressure-gradient, and the pressure-hessian tensor in an unforced, incompressible, homogeneous, and isotropic turbulent fluid. We exhibit several new results, including plots of the probability distributions of the spatial pressure-difference, the pressure-gradient norm, and the eigenvalues of the pressure-hessian tensor, temporal evolution of the mean pressure-hessian eigenvalues and of the mean pressure-gradient norm, as well as isosurfaces of the pressure and the pressure-gradient norm, at cascade completion. Statistical properties of the non-local part of the pressure-hessian tensor are also exhibited, for the first time. We construct the general alignment picture between the eigenvectors of the pressure-hessian tensor, the pressure-gradient, the eigenvectors of the strain-rate tensor, the vorticity, and the velocity. Ohkitani[13] and Ohkitani and Kishiba[14] have derived several interesting results for the unforced, incompressible, three-dimensional, inviscid Navier-Stokes equations (the Euler equations) concerning the pressure-hessian and the strain-rate tensors. We exhibit numerical tests of some conjectures for the Navier-Stokes case.

---

\*Electronic address: kalelkar@physics.iisc.ernet.in

The unforced Navier-Stokes equations are

$$\frac{\partial \mathbf{v}}{\partial t} + (\mathbf{v} \cdot \nabla) \mathbf{v} = -\frac{\nabla p}{\rho} + \nu \nabla^2 \mathbf{v}, \quad (1)$$

where  $\nu$  is the kinematic viscosity,  $\rho$  is the (constant) density, and  $p$  is the pressure. On taking the divergence of Eqs. (1), and enforcing incompressibility  $\nabla \cdot \mathbf{v} = 0$ , the pressure is determined by

$$\nabla^2 p = \left( \frac{1}{2} \omega^2 - s^2 \right) \rho, \quad (2)$$

where the enstrophy  $\omega^2 = \omega_i \omega_i$ ,  $\omega_i \equiv \epsilon_{ijk} \partial_j v_k$  is the vorticity ( $\epsilon_{ijk}$  is the Levi-Civita tensor),  $i, j, k = 1, 2, 3$ , with a summation implicit over repeated indices, and  $s^2 = S_{ij} S_{ij}$ ,  $S_{ij} \equiv 1/2(\partial_j v_i + \partial_i v_j)$  is the strain-rate tensor.

## II. NUMERICAL METHOD

We use a pseudospectral method[15] to solve Eqs. (1) numerically, in a cubical box of side  $2\pi$  with periodic boundary conditions and  $224^3$  Fourier modes. In this paper, we do not address issues pertaining to the scaling of higher-order structure functions of the pressure-difference (or pressure-velocity correlations) or investigate dissipation-scale properties, and believe that our spectral resolution is adequate for the types of studies that we have carried out (barring the pressure spectrum, see below). We have checked that our results are unaffected by resolution considerations, by comparing with results from a  $128^3$  DNS study with identical (initial) Reynolds number. For the temporal evolution, we use an Adams-Bashforth scheme (step size  $\delta t = 10^{-3}$ ) with double-precision arithmetic and set  $\rho = 1$ ,  $\nu = 10^{-5}$ . We include a hyperviscous term of the form  $\nu_h \nabla^4 \mathbf{v}$  in Eqs. (1), with  $\nu_h = 10^{-6}$  and have explicitly checked that our results are unaffected by the inclusion of hyperviscosity. We note that Borue and Orszag[16] have carried out a  $256^3$  DNS study of decaying, isotropic turbulence with hyperviscosity, and they conclude that "...inertial-range dynamics may be independent of the particular mechanism of small-scale dissipation..." (p. R859, Ref. [16]). The initial velocity field is taken to be  $\mathbf{v}(\mathbf{k}, t_0) \sim k^2 e^{-k^2} e^{i\theta_{\mathbf{k}}}$  ( $k = |\mathbf{k}|$  is the wavenumber), with  $\theta_{\mathbf{k}}$  independent random variables distributed uniformly between 0 and  $2\pi$ . This corresponds to an initial kinetic-energy spectrum  $E(k, t_0) \sim k^4 e^{-2k^2}$  (with  $E(k, t) \equiv |\mathbf{v}(\mathbf{k}, t)|^2$  the one-dimensional spectrum), which is a convenient choice that develops a cascade to large wavenumbers (see below). We measure time in units of the initial 'box-size' time  $\tau_0 \equiv 2\pi/v_{rms}^0$  (here  $\tau_0$  equals 4.02),  $v_{rms}^0 \equiv [(\sum_{\mathbf{k}} |\mathbf{v}(\mathbf{k}, t_0)|^2)]^{1/2}$  is the root-mean-square value of the initial velocity, with the dimensionless time  $\tau \equiv t/\tau_0$  ( $t$  is the product of the number of steps and  $\delta t$ ). We define  $Re_0 \equiv 2\pi v_{rms}^0/\nu$  to be the value of the initial 'box-size' Reynolds number (here  $Re_0$  equals

982464). Our results are obtained for times  $t_0 \leq t \ll t_*$ , where  $t_*$  is the time at which the (growing) integral scale  $L(t) \equiv \langle (\sum_{\mathbf{k}} |\mathbf{v}(\mathbf{k}, t)|^2/k) / \sum_{\mathbf{k}} |\mathbf{v}(\mathbf{k}, t)|^2 \rangle$  becomes of the order of the linear size of the simulation box. For times  $t \gtrsim t_*$ , finite-size effects which might well be non-universal, modify the numerical results, and are not considered here.

In Fig. 1, we show some preliminary results that serve as a check of our numerical method and parameter values (which were chosen to ensure linear stability of the numerical scheme). Figure 1(a) shows on a log-log plot, the scaled kinetic energy spectrum  $k^{5/3} E(k, \tau)$  as a function of the wavenumber  $k$ . On starting with the spectrum specified above, a cascade of energy is seen to large wavenumbers. The plots are equispaced in time with a temporal separation of  $\tau = 0.24$ . The plot with open circles is calculated at cascade completion at the dimensionless time  $\tau = \tau_c = 0.71$ , and shows a wavenumber range (for  $1 \lesssim k \lesssim 10$ ) that exhibits the well-known  $-5/3$  power-law[11, 17, 18]. Upon cascade completion, the shape of the energy spectrum does not change appreciably (except at large wavenumbers where it falls), but the kinetic energy decays monotonically. In Fig. 1(b), we plot the normalized kinetic energy-dissipation rate  $\epsilon(\tau)/\epsilon_0$  [ $\epsilon(t) \equiv \sum_{\mathbf{k}} k^2 |\mathbf{v}(\mathbf{k}, t)|^2$ ] as a function of the dimensionless time  $\tau$ . The kinetic energy-dissipation rate peaks[17, 18] at  $\tau = \tau_c$ , corresponding to cascade completion in the kinetic energy spectrum, and decreases thereafter. The turbulence may be considered as 'fully developed' at  $\tau = \tau_c$  and our spatial results (see below) will be calculated at this instant of time.

## III. NUMERICAL RESULTS

### A. Pressure

At each grid point, we compute  $p$  by Fourier-transforming Eq. (2), solving for the pressure, and inverse Fourier-transforming to physical space. Kolmogorov phenomenology predicts that the pressure spectrum in statistically steady turbulence exhibits a wavenumber range with the power-law scaling  $p(k) \sim k^{-7/3}$ [11]. Ishihara, *et.al.*[4] have confirmed the scaling law in a  $2048^3$  DNS study of statistically steady, homogeneous, and isotropic turbulence at a Taylor-scale Reynolds number  $Re_\lambda = 732$ , whereas Tsuji and Ishihara[19] have observed the scaling law by measuring pressure fluctuations in the centre line of a freely decaying turbulent jet. In Fig. 2(a), we plot the scaled pressure spectrum  $k^{7/3} p(k, \tau)$  as a function of the wavenumber  $k$ , at cascade completion. In order to observe Kolmogorov-type scaling in the pressure spectrum over a substantial wavenumber range, a considerably higher (initial) Reynolds number is required[20] as compared to the result for the kinetic-energy spectrum [cf. plot with open circles in Fig. 1(a)]. The spectral resolution of our study is inadequate for the purposes of fitting a power-law, and

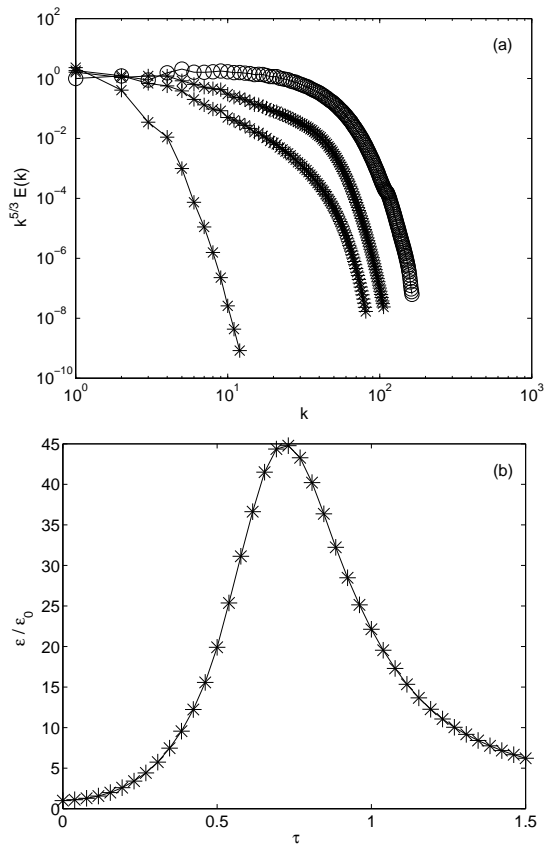


FIG. 1: (a) Log-log plot of the temporal evolution of the scaled kinetic energy spectrum  $k^{5/3}E(k, \tau)$  as a function of the wavenumber  $k$  at temporal separations of  $\tau = 0.24$ . The plot with open circles is calculated at cascade completion, at dimensionless time  $\tau = \tau_c = 0.71$ . (b) Plot of the normalized kinetic energy-dissipation rate  $\epsilon(\tau)/\epsilon_0$  as a function of the dimensionless time  $\tau$ .

the pressure spectrum is found to exhibit a  $-7/3$  power-law only in the narrow wavenumber range  $20 \lesssim k \lesssim 50$ .

In Fig. 2(b), we plot the normalized probability distribution  $\mathcal{P}(\Delta p_r)$  of the pressure-difference  $\Delta p_r \equiv p(\mathbf{x} + \mathbf{r}) - p(\mathbf{x})$  at cascade completion, for grid-spacing values  $r \equiv |\mathbf{r}| = 1, 50$ . For the large separation  $r = 50$ ,  $\mathcal{P}(\Delta p_{50})$  is found to be close to a Gaussian distribution [cf. dashed-line curve in Fig. 2(b)] with a skewness equal to zero, and a kurtosis equal to 3.49. For  $r = 1$ , stretched-exponential tails which are roughly symmetrically placed about  $\Delta p_1 = 0$  are observed, with  $\mathcal{P}(\Delta p_1)$  having a kurtosis equal to 7.80. We note that  $\mathcal{P}(\Delta p_1)$  does not exhibit a Gaussian core at small values of  $\Delta p_1/\sigma$  ( $\sigma$  is the standard deviation). Our results for  $\mathcal{P}(\Delta p_r)$  resemble those obtained for probability distribution of the spatial velocity-difference[21] at large and small grid-spacings respectively. Cao, *et.al.*[2] obtained similar results for  $\mathcal{P}(\Delta p_r)$  from a  $512^3$  DNS study of statistically steady, homogeneous, and isotropic turbulence at  $Re_\lambda = 218$ .

In Fig. 3(a), we plot the normalized probability distribution  $\mathcal{P}(p)$  of  $p$ , at cascade completion. The mean pres-

sure  $\langle p \rangle$  (angular brackets denote a volume average) was found to equal zero, as is expected[11] for isotropic turbulence, whereas the skewness was found to equal  $-0.11$  and the kurtosis equalled 5.62. Holzer and Siggia[22] have shown analytically, that the probability distribution of the pressure is negatively skewed and has an exponential tail, for a *Gaussian*[23] velocity probability distribution. Brachet[24] has found a low-pressure exponential tail in an  $864^3$  DNS study of decaying, isotropic turbulence with Taylor-Green[25] initial conditions. The error bars in this study[24] are probably larger than those in the data of Fig. 3(a). Both Pumir[1] and Cao, *et.al.*[2] observed a stretched-exponential tail at low pressures, and a roughly Gaussian tail at high pressures, in DNS studies of  $p$  in statistically steady turbulence. We confirm the result for negative pressures in the case of decaying turbulence, where the fit  $\mathcal{P}(|p|) \sim e^{-\beta|p|^\alpha}$ ,  $\beta = 2.55 \pm 0.01$ ,  $\alpha = 1.35 \pm 0.01$  (error-bars from least-square fits), is observed at cascade completion. However, at positive pressures, a stretched-exponential tail with  $\beta = 1.80 \pm 0.01$ ,  $\alpha = 1.52 \pm 0.02$  (error-bars from least-square fits) is observed in our study.

In Fig. 3(b), we plot iso- $p$  surfaces for the isovalue  $p = \langle p \rangle$  at cascade completion, which appear to be crumpled sheet-like structures (found throughout the isovalue range  $[\langle p \rangle - \sigma, \langle p \rangle + \sigma]$ ). Equation (2) suggests that regions with high vorticity and low strain-rates are simultaneously sources of low pressure. Such regions with intense vorticity have been observed by Douady, *et.al.*[9] and Villermaux, *et.al.*[10] in statistically steady turbulence experiments, by using cavitation as a visualization technique, in a liquid seeded with bubbles. Schumann and Patterson[12] exhibited plots of low-pressure isosurfaces from a  $32^3$  DNS study of the unforced, incompressible, three-dimensional Navier-Stokes equations, which were shown to be organised as ‘cloud’-like structures. In our study, at early times  $\tau \ll \tau_c$ , regions of low pressure (with the isovalue  $p = \langle p \rangle - 2\sigma$ ) are found to be sheet-like [see Fig. 4(a)]. At cascade completion, low-pressure regions are found to be organised as slender filaments [see Fig. 4(b)], with diameter of the order of the grid spacing, and a contour length that occasionally extends nearly to the linear size of the simulation box. We choose to quote dimensions of the structures relative to the (fixed) box-size and the grid-spacing, since both the Kolmogorov (dissipative) and the integral length scales vary in time, in decaying turbulence. Isosurface plots of the enstrophy and the squared strain-rates show (see Ref. [2]) that highly-strained regions occur close to regions of intense enstrophy, and Eq. (2) suggests a lack of any well-defined fluid-mechanical structure of the high-pressure regions. In our study, iso- $p$  surfaces in the range  $p > (\langle p \rangle + \sigma)$  were indeed found not to exhibit any particular structure at cascade completion.

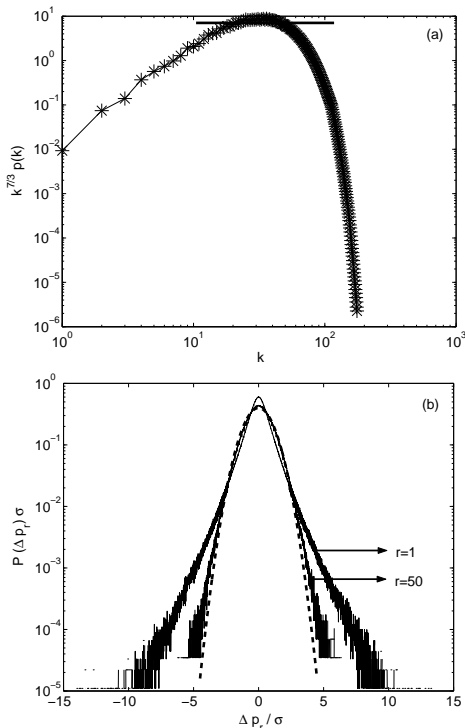


FIG. 2: (a) Log-log plot of the scaled pressure spectrum  $k^{7/3}p(k, \tau)$  as a function of the wavenumber  $k$ , at cascade completion. The horizontal line is drawn for reference. (b) Semilog plot of the normalized probability distribution  $\mathcal{P}(\Delta p_r)$  ( $\sigma$  is the standard deviation) of the pressure-difference  $\Delta p_r$  at cascade completion, for grid-spacing values  $r = 1, 50$ . The dashed-line curve is a normalized Gaussian distribution for comparison.

## B. Pressure-Hessian Tensor

The pressure-hessian tensor  $P_{ij} \equiv \partial_{ij}p$  appears[13, 14] in the evolution equation for the strain-rate tensor  $S_{ij}$ . At each grid point, we compute the eigenvalues  $\lambda_{1,P}$ ,  $\lambda_{2,P}$ , and  $\lambda_{3,P}$  (with the convention  $\lambda_{1,P} \geq \lambda_{2,P} \geq \lambda_{3,P}$ ) of  $P_{ij}$  and the corresponding orthonormal eigenvectors  $f_1$ ,  $f_2$ , and  $f_3$ . We also compute the eigenvalues  $\lambda_{1,S}$ ,  $\lambda_{2,S}$ , and  $\lambda_{3,S}$  (with ordering from extensional to compressive strain-rates  $\lambda_{1,S} \geq \lambda_{2,S} \geq \lambda_{3,S}$ ) of  $S_{ij}$  and the corresponding orthonormal eigenvectors  $e_1$ ,  $e_2$ , and  $e_3$ .

In Fig. 5(a), we plot the normalized probability distribution  $\mathcal{P}(\lambda_{i,P})$  of the eigenvalues  $\lambda_{i,P}$ , at cascade completion. The skewnesses of the eigenvalue distributions were found to equal 4.73, 5.25, and  $-4.13$  for  $i = 1, 2$ , and 3 respectively.

In a constant-density flow, incompressibility requires that  $\sum_i \lambda_{i,S} = 0$ , however, there is no such constraint on  $\lambda_{i,P}$ . The inset plot in Fig. 5(b) is the normalized probability distribution of the trace of  $P_{ij}$ ,  $\mathcal{P}[x = Tr(P_{ij})]$  ( $Tr(P_{ij}) \equiv \sum_k \lambda_{k,P}$ ) at cascade completion, which is roughly symmetrically placed about  $x = 0$ . As is well-known in both decaying[18] and statistically steady[21] turbulence, regions of intense vorticity (say, for iso- $|\omega|$

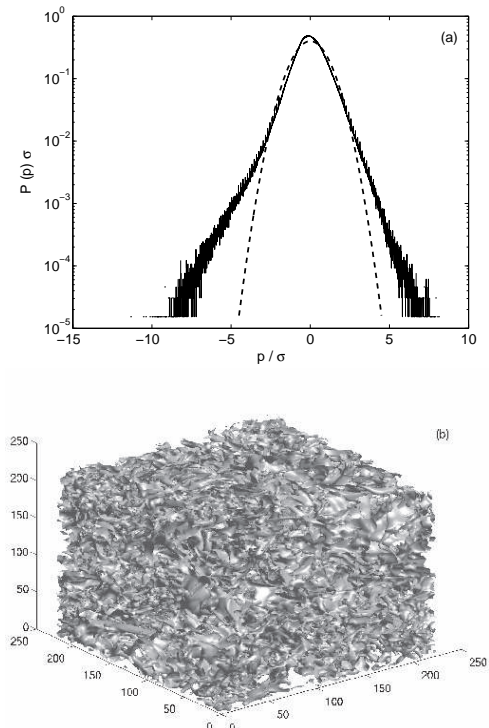


FIG. 3: (a) Semilog plot of the normalized probability distribution  $\mathcal{P}(p)$  of the pressure  $p$ , at cascade completion. The dashed-line curve is a normalized Gaussian distribution for comparison. (b) Plot of iso- $p$  surfaces for the isovalue  $p = \langle p \rangle$ , at cascade completion.

values greater than  $(\langle |\omega| \rangle + 2\sigma)$  are found to be organized as filamentary structures, and are spatially more localized than regions of high strain-rate. Equation (2) suggests that locally, in regions of intense enstrophy,  $Tr(P_{ij}) = \nabla^2 p > 0$ . In Fig. 5(b), we plot the normalized probability distribution  $\mathcal{P}[Tr(P_{ij})]$  of the trace of  $P_{ij}$  at cascade completion conditioned on  $|\omega| \geq \langle |\omega| \rangle + 2\sigma$ , which is found to have a positive mean as expected.

Ohkitani and Kishiba[14], have shown that the pressure-hessian tensor  $P_{ij}$  can be decomposed into the sum of a diagonal tensor  $\delta_{ij} \nabla^2 p / 3$  (the ‘local’ term),  $\delta_{ij}$  is the Kronecker delta, and a symmetric, zero-diagonal tensor  $Q_{ij}$ [27] (the ‘non-local’ term). The local term, as the name indicates, can be expressed purely in terms of the vorticity and the strain-rate at each point of the fluid [see Eq. (2)], however, the non-local term can be expressed only in terms of an integral over the entire fluid volume. Ohkitani and Kishiba[14] have also shown (for Taylor-Green[25] initial conditions) that the non-local term contributes significantly to enstrophy growth. Since  $Q_{ij} = P_{ij} - \delta_{ij} \nabla^2 p / 3$  has zero trace, its eigenvalue  $\lambda_{1,Q} > 0$ ,  $\lambda_{3,Q} < 0$ , and the sign of  $\lambda_{2,Q}$  is indeterminate. In Fig. 5(c), we plot the normalized probability distribution  $\mathcal{P}(\lambda_{i,Q})$  of the eigenvalues  $\lambda_{i,Q}$ , at cascade completion. We find that  $\lambda_{2,Q}$  has a positive mean. The statistically preferred ratio of the mean eigenvalues

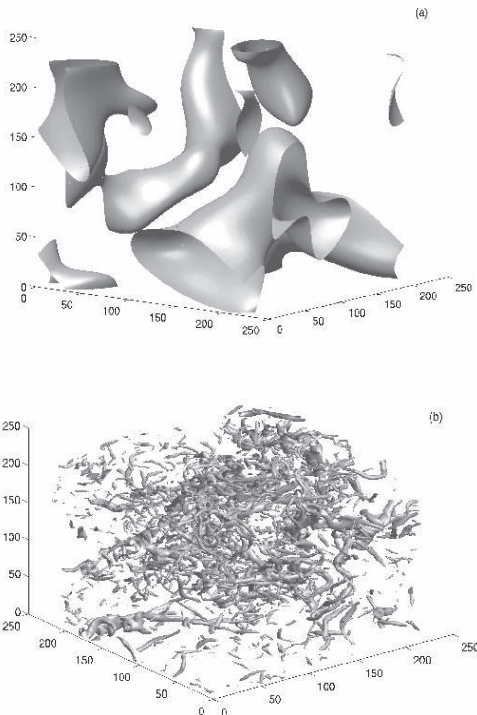


FIG. 4: (a) Plot of iso- $p$  surfaces for the isovalue  $p = \langle p \rangle - 2\sigma$  at the dimensionless time  $\tau \ll \tau_c$ . (b) Plot of iso- $p$  surfaces for the isovalue  $p = \langle p \rangle - 2\sigma$ , at cascade completion.

$\langle \lambda_{1,Q} \rangle : \langle \lambda_{2,Q} \rangle : \langle \lambda_{3,Q} \rangle$  was found to equal  $46 : 1 : -47$ , at cascade completion[26].

In Fig. 6(a), we plot the mean eigenvalues  $\langle \lambda_{i,P} \rangle$  as a function of the dimensionless time  $\tau$ , these evolve in a way that is similar to the temporal evolution of the kinetic-energy dissipation rate, with a peak in the magnitude of  $\langle \lambda_{i,P} \rangle$ , at cascade completion [cf. Fig. 1(b)]. Similar results (not shown here) were obtained for the temporal evolution of  $\langle \lambda_{i,Q} \rangle$ . Ohkitani[13], in a  $128^3$  DNS study of the unforced, incompressible, three-dimensional Euler equations, showed that  $\lambda_{3,P}$  changes sign (locally, in regions of intense enstrophy) from positive to negative at early times. However, in our study, we find that  $\langle \lambda_{2,P} \rangle$  changes sign [see Fig. 6(b)] at  $\tau = 0.37$  from negative to positive, whereas  $\langle \lambda_{3,P} \rangle$  remains negative at all times (not shown here).

In Fig. 7(a), we plot the normalized probability distribution of the cosines of the angles between the eigenvectors  $f_i$  of  $P_{ij}$ [28] and the pressure-gradient  $\nabla p$  (see below), at cascade completion. In Fig. 7(b), we plot the normalized probability distribution of the cosines of the angles between the eigenvectors  $f_i$  and  $\omega$ , at cascade completion. Ohkitani[13] showed that  $\omega$  is preferentially parallel (or anti-parallel) to the eigenvector  $f_3$  corresponding to the pressure-hessian eigenvalue  $\lambda_{3,P}$  smallest in magnitude, in contrast to our result, which shows that  $\omega$  is preferentially parallel (or anti-parallel) with the eigenvector  $f_2$  corresponding to the *intermediate* eigenvalue  $\lambda_{2,P}$ .

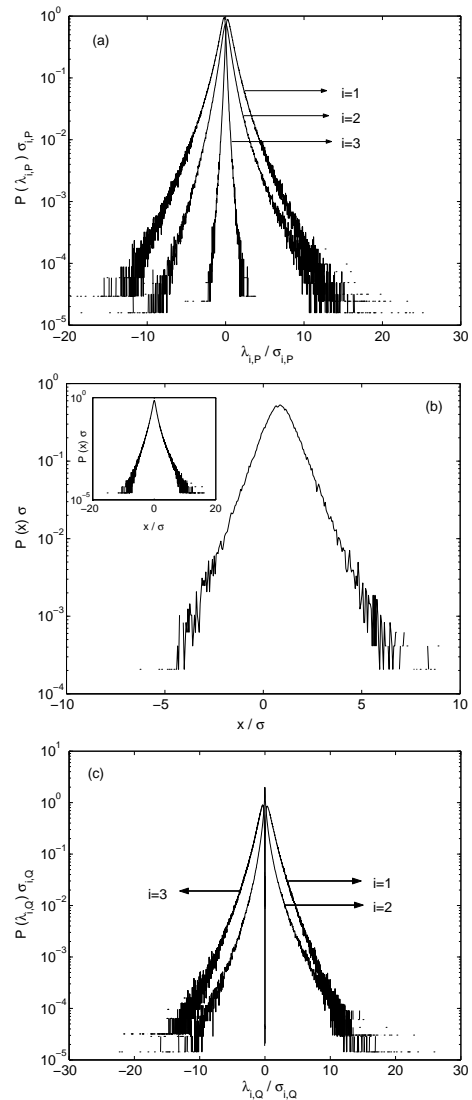


FIG. 5: (a) Semilog plot of the normalized probability distribution  $\mathcal{P}(\lambda_{i,P})$  of the eigenvalues  $\lambda_{i,P}$  of the pressure-hessian tensor  $P_{ij}$ , at cascade completion. (b) Semilog plot of the normalized probability distribution  $\mathcal{P}[x = Tr(P_{ij})]$  of the trace of  $P_{ij}$  ( $Tr(P_{ij}) \equiv \sum_k \lambda_{k,P}$ ) at cascade completion, conditioned on  $|\omega| \geq \langle |\omega| \rangle + 2\sigma$ . The inset is a semilog plot of the normalized probability distribution  $\mathcal{P}(x)$  of  $x = Tr(P_{ij})$ , at cascade completion. (c) Semilog plot of the normalized probability distribution  $\mathcal{P}(\lambda_{i,Q})$  of the eigenvalues  $\lambda_{i,Q}$  of the tensor  $Q_{ij}$  (see the text for the definition), at cascade completion.

In Fig. 7(c), we plot the normalized probability distribution of the cosines of the angles between the eigenvectors  $f_i$  and the velocity  $\mathbf{v}$ , at cascade completion.

### C. Pressure Gradient

A systematic numerical study of the pressure gradient is entirely lacking in both statistically steady and decay-

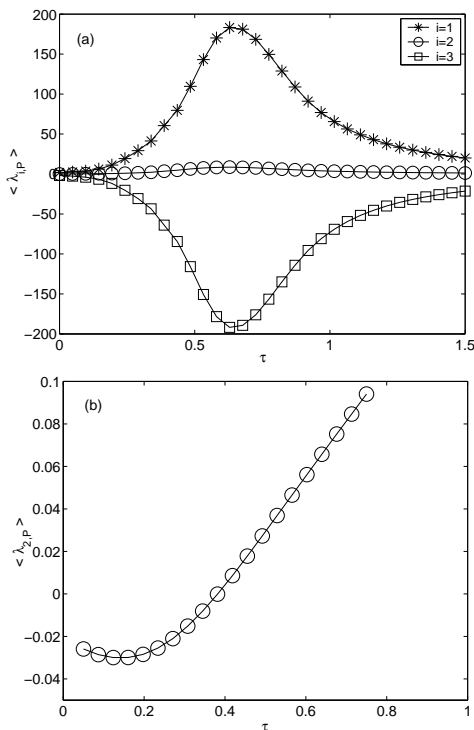


FIG. 6: (a) Plot of the mean eigenvalues  $\langle \lambda_{i,P} \rangle$  of  $P_{ij}$  as a function of the dimensionless time  $\tau$ . (b) Plot of  $\langle \lambda_{2,P} \rangle$  as a function of the dimensionless time  $\tau$ , in the range  $0 < \tau \le 0.75$ .

ing turbulence. In Fig. 8(a), we plot the normalized probability distribution  $\mathcal{P}(|\nabla p|)$  of the Euclidean norm ( $|\mathbf{x}| \equiv \sqrt{\sum_i x_i^2}$  for vector  $\mathbf{x}$  with components  $x_i$ ) of the pressure-gradient  $\nabla p$  at cascade completion, which does not exhibit a stretched-exponential tail. The author has been unable to determine a functional form which gives a good fit for the tail of  $\mathcal{P}(|\nabla p|)$ .

In Fig. 8(b), we plot the mean pressure-gradient norm  $\langle |\nabla p| \rangle$  as a function of the dimensionless time  $\tau$ , which is observed to peak at  $\tau = \tau_c$ , as does the kinetic-energy dissipation rate [see Fig. 1(b)].

In Fig. 8(c), we plot iso- $|\nabla p|$  surfaces for the isovalue  $|\nabla p| = \langle |\nabla p| \rangle + 2\sigma$ , at cascade completion. The iso-surfaces of intense pressure-gradient, which are filamentary in shape, are found to resemble the *low*-pressure isosurfaces in Fig. 4(b). Iso- $|\nabla p|$  surfaces in the range  $|\nabla p| < (\langle |\nabla p| \rangle - \sigma)$  were not found to exhibit any particular structure at cascade completion.

In Fig. 9(a), we plot the normalized probability distribution of the cosines of the angles between  $\nabla p$  and the eigenvectors  $e_i$  of  $S_{ij}$ . Ashurst, *et.al.*[5], noted a tendency for the alignment of  $\nabla p$  (caused by velocity fluctuations alone) with the most compressive strain direction  $e_3$  in a  $128^3$  DNS study of a statistically steady turbulent shear-flow. However, in our study,  $\nabla p$  is not found to be preferentially parallel (or anti-parallel) with  $e_3$ , and we observe a peak in the magnitude of  $\mathcal{P}[\cos(\nabla p, e_3)]$

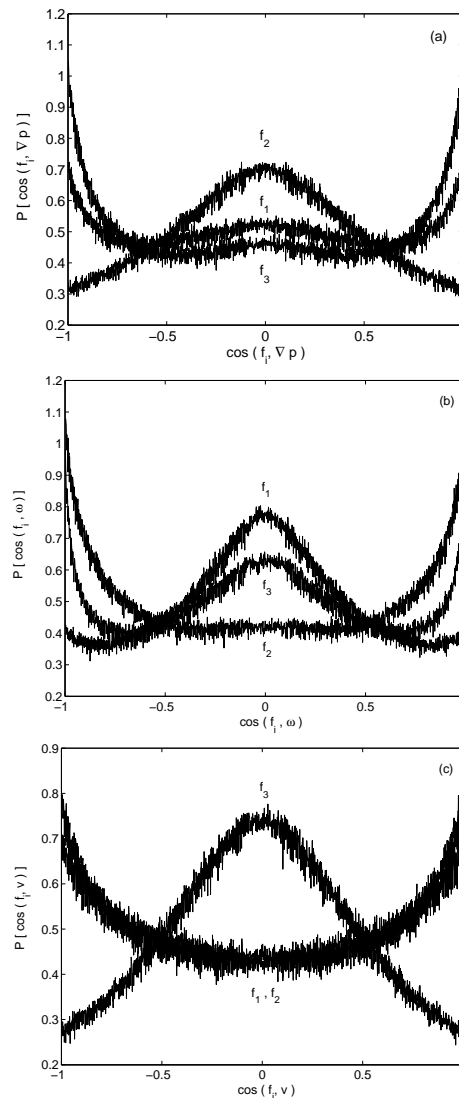


FIG. 7: (a) Plot of the normalized probability distribution of the cosines of the angles between the eigenvectors  $f_i$  of  $P_{ij}$  and the pressure gradient  $\nabla p$ , at cascade completion. (b) Plot of the normalized probability distribution of the cosines of the angles between the eigenvectors  $f_i$  and the vorticity  $\omega$ , at cascade completion. (c) Plot of the normalized probability distribution of the cosines of the angles between the eigenvectors  $f_i$  and the velocity  $\mathbf{v}$ , at cascade completion.

at  $|\cos(\nabla p, e_3)| \approx 0.86$ , which indicates a preferential relative angle  $\approx \pi/6$ . In Fig. 9(b), we plot the normalized probability distribution of the cosine of the angle between  $\nabla p$  and  $\omega$ , at cascade completion. In Fig. 9(c), we plot the normalized probability distribution of the cosine of the angle between  $\nabla p$  and  $\mathbf{v}$ , at cascade completion. Both  $\omega$  and  $\mathbf{v}$  are observed to be preferentially perpendicular to  $\nabla p$ , in agreement with corresponding results from a  $128^3$  DNS study of the unforced, incompressible, three-dimensional Euler equations, due to Ohkitani and Kishiba[14].

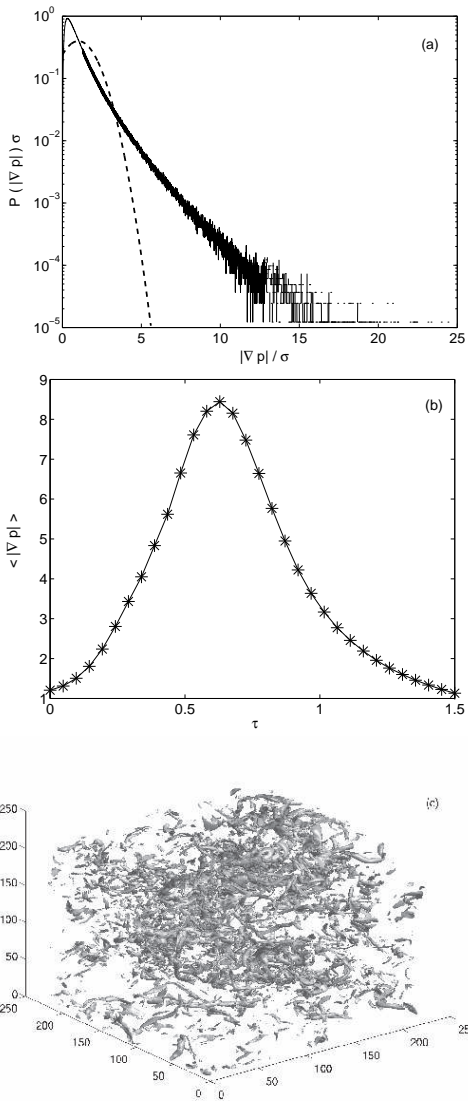


FIG. 8: (a) Semilog plot of the normalized probability distribution  $\mathcal{P}(|\nabla p|)$  ( $|\nabla p|$  is the Euclidean norm of the pressure-gradient), at cascade completion. The dashed-line curve is a normalized Gaussian distribution for comparison. (b) Plot of the mean pressure-gradient norm  $\langle |\nabla p| \rangle$  as a function of the dimensionless time  $\tau$ . (c) Plot of iso- $|\nabla p|$  surfaces for the isovalue  $|\nabla p| = \langle |\nabla p| \rangle + 2\sigma$ , at cascade completion.

#### D. General Alignment Picture

Ohkitani and Kishiba[14] have found the orientations (locally, in regions of intense enstrophy) amongst the set of vectors  $(e_i, f_i, \omega)$ , excluding the pressure gradient and the velocity. In Figs. 7 and 9, we have plotted possible alignments between the sets of vectors  $(f_i, \nabla p)$  and  $(e_i, \mathbf{v}, \omega)$  and for completeness, we plot in Figs. 10 and 11, remaining alignments amongst the set of vectors  $(e_i, \mathbf{v}, \omega)$  and amongst the eigenvector bases  $(f_i, e_i)$ , at cascade completion.

As is well-known, in both decaying[18] and statisti-

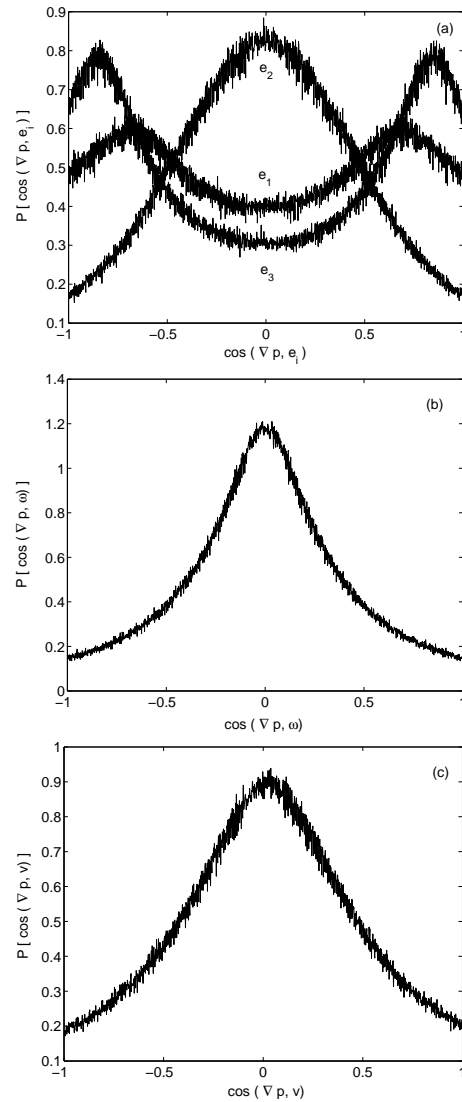


FIG. 9: (a) Plot of the normalized probability distribution of the cosines of the angles between  $\nabla p$  and the eigenvectors  $e_i$  of the strain-rate tensor  $S_{ij}$ , at cascade completion. (b) Plot of the normalized probability distribution of the cosine of the angle between  $\nabla p$  and  $\omega$ , at cascade completion. (c) Plot of the normalized probability distribution of the cosine of the angle between  $\nabla p$  and  $\mathbf{v}$ , at cascade completion.

cally steady[21] turbulence, there is an increased probability for alignment (or anti-alignment) of the intermediate strain-rate eigenvector  $e_2$  with  $\omega$ , relative to the alignments between  $e_1$  and  $e_3$  with  $\omega$ . In Fig. 10(a), we plot the normalized probability distribution of the cosines of the angles between  $\omega$  and  $e_i$  at cascade completion, which reaffirms this result for decaying turbulence. In Fig. 10(b), we plot the normalized probability distribution of the cosines of the angles between  $\mathbf{v}$  and  $e_i$ , at cascade completion. In Fig. 10(c), we plot the normalized probability distribution of the cosine of the angle between  $\mathbf{v}$  and  $\omega$ , at cascade completion. It is interesting to note that the alignment plots in Figs. 7, 9, and 10(a),(b)



are roughly symmetrically placed about  $\cos\theta = 0$ , however Fig. 10(c) is distinctly asymmetric, with a greater probability for  $\mathbf{v}$  and  $\omega$  to be *anti*-parallel. This asymmetry has been noted in a laboratory experiment[29] of decaying turbulent flow past a grid, and is plausibly due to effects of the kinetic helicity[30] (an invariant of the Euler equations) on the decay process.

In Fig. 11(a),  $\mathcal{P}[\cos(f_1, e_1)]$  is found to peak at  $|\cos(f_1, e_1)| \approx 0.71$ , which indicates a preferential relative angle  $\approx \pi/4$ , in agreement with corresponding results due to Ohkitani and Kishiba[14]. The only distinct feature in Figs. 11(b),(c) is that  $f_2$  is preferentially parallel (or anti-parallel) to  $e_2$  (and perpendicular to  $e_3$ ).

Ohkitani[13] has conjectured that the pressure-hessian tensor  $P$  (with components  $P_{ij}$ ) and the strain-rate tensor  $S$  (with components  $S_{ij}$ ) in general are *not* commutative, and therefore cannot be simultaneously diagonalized. It is of interest to determine the (statistically preferred) relative orientation, between the two frames with respect to which  $S$  and  $P$  are diagonalized. Ohkitani and Kishiba[14] have conjectured that the configuration of relative alignments between the eigenvector bases  $(f_i, e_i)$  is one with “least commutativity between  $S$  and  $P$  out of all possibilities with one axis in common” (p. 414, Ref. [14]) at cascade completion. In order to test these conjectures, we choose the standard matrix norm  $\|A\| = (\text{maximum eigenvalue of } A^T A)^{1/2}$ [31], where the superscript  $T$  denotes the transpose-conjugate. In Fig. 12, we plot the mean norm  $\langle \| [S, P] \| \rangle$  of the commutator  $[S, P] = SP - PS$ [32] as a function of the dimensionless time  $\tau$  and find that the value peaks at  $\tau = 0.71$ . The *value* of the mean norm depends on the choice of the norm; however, the trend (which is independent of this choice) indicates that the relative configuration of the eigenvector bases  $(f_i, e_i)$  is “least commutative” at  $\tau = 0.71$ , which is equal to the time at which the kinetic energy-dissipation rate peaks, in accord with the Ohkitani and Kishiba[14] conjecture.

#### IV. CONCLUSION

To summarize, we have presented results from a systematic numerical study of pressure fluctuations in an unforced, incompressible, homogeneous, and isotropic turbulent fluid. At cascade completion, isosurfaces of low pressure are found to be organised as slender filaments, whereas the predominant pressure isostructures appear sheet-like. We have exhibited several new results, including plots of the probability distributions of the spatial pressure-difference, the pressure-gradient norm, and the eigenvalues of the pressure-hessian tensor, at cascade completion. Plots of the temporal evolution of the mean pressure-gradient norm, and the mean eigenvalues of the pressure-hessian tensor have also been exhibited. We have found the statistically preferred orientations between the eigenvectors of the pressure-hessian tensor, the pressure-gradient, the eigenvectors of the strain-rate ten-

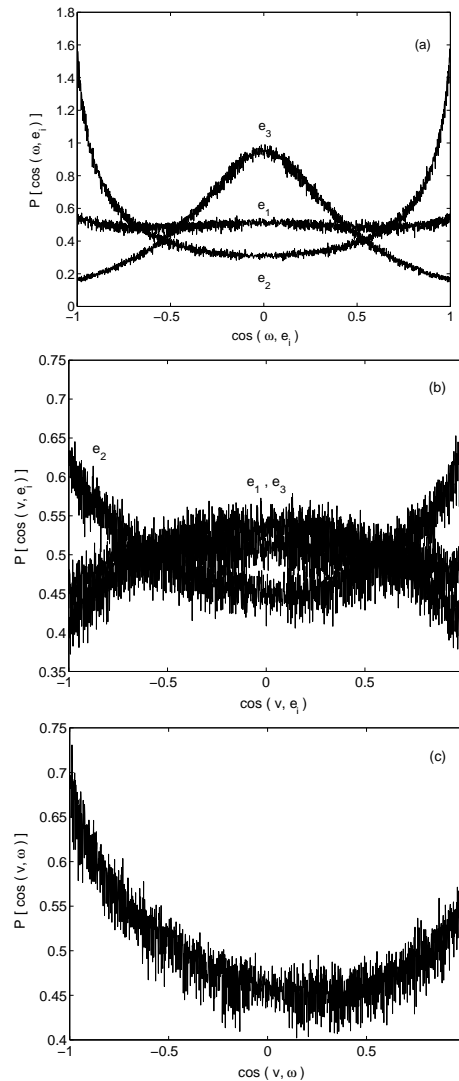


FIG. 10: (a) Plot of the normalized probability distribution of the cosines of the angles between  $\omega$  and the eigenvectors  $e_i$ , at cascade completion.

(b) Plot of the normalized probability distribution of the cosines of the angles between  $\mathbf{v}$  and the eigenvectors  $e_i$ , at cascade completion.

(c) Plot of the normalized probability distribution of the cosine of the angle between  $\mathbf{v}$  and  $\omega$ , at cascade completion.

sor, the vorticity, and the velocity at cascade completion. Statistical properties of the non-local part of the pressure-hessian tensor have also been exhibited, for the first time. We have presented numerical tests (in the viscous case) of some conjectures for the unforced, incompressible, three-dimensional Euler equations, proposed in earlier studies.



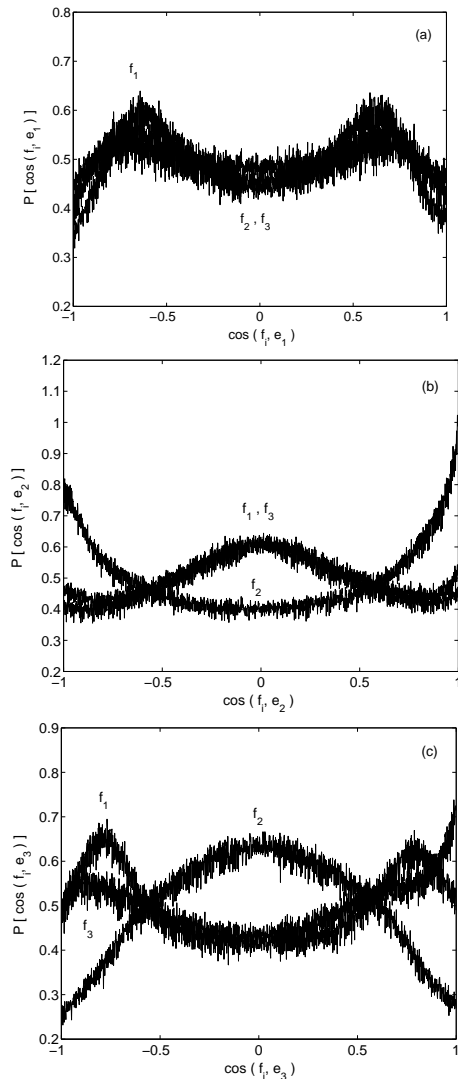


FIG. 11: (a) Plot of the normalized probability distribution of the cosines of the angles between the eigenvectors  $f_i$  and  $e_1$ , at cascade completion. (b) Plot of the normalized probability distribution of the cosines of the angles between the eigenvectors  $f_i$  and  $e_2$ , at cascade completion. (c) Plot of the normalized probability distribution of the cosines of the angles between the eigenvectors  $f_i$  and  $e_3$ , at cascade completion.

## V. ACKNOWLEDGEMENT

The author thanks T. Kalelkar and R. Pandit for discussions, D. Mitra for the code, SERC (IISc) for computational resources, and CSIR (India) for financial support.

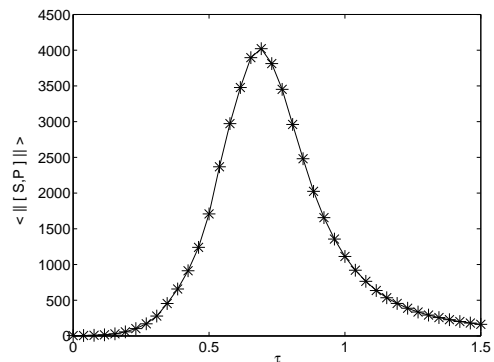


FIG. 12: Plot of the mean norm  $\langle ||[S, P]|| \rangle$  (see the text for the definition of the norm) of the commutator  $[S, P] = SP - PS$  of the strain-rate  $S$  and the pressure-hessian  $P$  tensors, as a function of the dimensionless time  $\tau$ .

[1] A. Pumir, Phys. Fluids **6**, 2071 (1994).  
 [2] N. Cao, S. Chen, and G. Doolen, Phys. Fluids **11**, 2235 (1999).  
 [3] T. Gotoh and D. Fukayama, Phys. Rev. Lett. **86**, 3775 (2001).  
 [4] T. Ishihara, Y. Kaneda, M. Yokokawa, K. Itakura, and A. Uno, J. Phys. Soc. Jpn. **72**, 983 (2003).  
 [5] W. Ashurst, J. Chen, and M. Rogers, Phys. Fluids **30**, 3293 (1987).  
 [6] Z. She, E. Jackson, and S. Orszag, Nature, **344**, 226

(1990); Z. She, E. Jackson, and S. Orszag, Proc. Roy. Soc. London, Ser. A, **434**, 101 (1991).  
 [7] S. Fauve, C. Laroche, and B. Castaing, J. Phys. II (France) **3**, 271 (1993).  
 [8] P. Abry, S. Fauve, P. Flandrin, and C. Laroche, J. Phys. II (France) **4**, 725 (1994).  
 [9] S. Douady, Y. Couder, and M. Brachet, Phys. Rev. Lett. **67**, 983 (1991).  
 [10] E. Villermaux, B. Sixou, and Y. Gagne, Phys. Fluids **7**, 2008 (1995).

- [11] A. Monin and A. Yaglom, *Statistical Fluid Mechanics*, edited by J. Lumley (MIT Press, Cambridge, 1975), Vol. **2**.
- [12] U. Schumann and G. Patterson, *J. Fluid Mech.* **88**, 685 (1978).
- [13] K. Ohkitani, *Phys. Fluids A* **5**, 2570 (1993).
- [14] K. Ohkitani and S. Kishiba, *Phys. Fluids* **7**, 411 (1995).
- [15] S. Dhar, A. Sain, and R. Pandit, *Phys. Rev. Lett.* **78**, 2964 (1997).
- [16] V. Borue and S. Orszag, *Phys. Rev. E*, **51**, R856 (1995).
- [17] K. Yamamoto and I. Hosokawa, *J. Phys. Soc. Jpn.* **57**, 1532 (1988).
- [18] C. Kalelkar, *Phys. Rev. E* **72**, 056307 (2005).
- [19] Y. Tsuji and T. Ishihara, *Phys. Rev. E* **68**, 026309 (2003).
- [20] M. Nelkin, *Adv. Phys.* **43**, 143 (1994).
- [21] A. Vincent and M. Meneguzzi, *J. Fluid Mech.* **225**, 1 (1991).
- [22] M. Holzer and E. Siggia, *Phys. Fluids A* **5**, 2525 (1993).
- [23] As is well-known (see Ref. [11] for instance), a Gaussian velocity probability distribution implies *zero* odd-order velocity correlations, in contradiction with numerical and laboratory results.
- [24] M. Brachet, *Fluid Dyn. Res.* **8**, 1 (1991).
- [25] G. Taylor and A. Green, *Proc. Roy. Soc. London, Ser. A* **158**, 499 (1937).
- [26] In Ref. [18], the statistically preferred ratio of the mean strain-rate eigenvalues  $\langle \lambda_{1,S} \rangle : \langle \lambda_{2,S} \rangle : \langle \lambda_{3,S} \rangle$  was found to equal  $5 : 1 : -6$ , at cascade completion.
- [27] From Ref. [14],  $Q_{ij}(\mathbf{x}) \equiv \oint q_{ij}(\mathbf{x} - \mathbf{y}) \nabla_y^2 p(\mathbf{y}) d\mathbf{y}$ ,  $q_{ij}(\mathbf{x}) = (|\mathbf{x}|^2 \delta_{ij} - 3x_i x_j) / (4\pi |\mathbf{x}|^5)$ ,  $\nabla_y^2 = \partial^2 / \partial y_i \partial y_i$ , where the integral is taken in the sense of principal values.
- [28] The alignment results for the eigenvectors of  $Q_{ij}$  were found to resemble those for  $f_i$ .
- [29] E. Kit, A. Tsinober, J. Balint, J. Wallace, and E. Levich, *Phys. Fluids* **30**, 3323 (1987).
- [30] R. Betchov, *Phys. Fluids* **4**, 925 (1961).
- [31] G. Strang, *Linear Algebra and its Applications*, (Thomson Learning, London, 1988).
- [32] The corresponding plot for  $[S, Q]$  is redundant since  $[S, Q] = [S, P]$ .